THE JOURNAL OF BIOLOGICAL CHEMISTRY VOL. 290, NO. 29, pp. 17710–17723, July 17, 2015

Oviductosome-Sperm Membrane Interaction in Cargo Delivery

*DETECTION OF FUSION AND UNDERLYING MOLECULAR PLAYERS USING THREE-DIMENSIONAL SUPER-RESOLUTION STRUCTURED ILLUMINATION MICROSCOPY (SR-SIM)**

Received for publication, December 17, 2014, and in revised form, May 11, 2015 Published, JBC Papers in Press, May 28, 2015, DOI 10.1074/jbc.M114.633156

Amal A. Al-Dossary[‡1], **Pradeepthi Bathala**[‡], **Jeffrey L. Caplan**[‡§], **and Patricia A. Martin-DeLeon**[‡2]

From the [‡]*Department of Biological Sciences, University of Delaware, Newark, Delaware 19716 and* [§]*Delaware Biotechnology Institute, Newark, Delaware 19711*

Background: The mechanism(s) for delivery of transmembrane proteins to sperm via exosomes/microvesicles is unknown.
Results: Using SR/SIM and a lipophilic dye, fusion detected for delivery of PMCA4 was inhibited by blocking integrin/ligand interactions.
Conclusion: Integrins on sperm and microvesicles play a role in microvesicle fusion for cargo delivery.
Significance: Delivery of reproductive microvesicle cargo that modulates fertility is mediated by integrins.

Oviductosomes ((OVS), exosomes/microvesicles), which deliver the Ca^{2+} efflux pump, plasma membrane Ca^{2+}ATPase 4 (PMCA4), to sperm are likely to play an important role in sperm fertilizing ability (Al-Dossary, A. A., Strehler, E. E., and Martin-DeLeon, P. A. (2013) *PloS one* 8, e80181). It is unknown how exosomes/microvesicles deliver transmembrane proteins such as PMCA4 to sperm. Here we define a novel experimental approach for the assessment of the interaction of OVS with sperm at a nanoscale level, using a lipophilic dye (FM4–64FX) and three-dimensional SR/SIM, which has an 8-fold increase in volumetric resolution, compared with conventional confocal microscopy. Coincubation assays detected fusion of prelabeled OVS with sperm, primarily over the head and midpiece. Immunofluorescence revealed oviductosomal delivery of PMCA4a to WT and *Pmca4* KO sperm, and also endogenous PMCA4a on the inner acrosomal membrane. Fusion was confirmed by transmission immunoelectron microscopy, showing immunogold particles in OVS, and fusion stalks on sperm membrane. Immunofluorescence colocalized OVS with the αv integrin subunit which, along with CD9, resides primarily on the sperm head and midpiece. In capacitated and acrosome reacted sperm, fusion was significantly ($p < 0.001$) inhibited by blocking integrin/ligand interactions via antibodies, exogenous ligands (vitronectin and fibronectin), and their RGD recognition motif. Our results provide evidence that receptor/ligand interactions, involving αvβ3 and α5β1integrins on sperm and OVS, facilitate fusion of OVS in the delivery of transmembrane proteins to sperm. The mechanism uncovered is likely to be also involved in cargo delivery of prostasomes, epididymosomes, and uterosomes.

Reproductive fluids of the male tract and uterine environment are known to contain extracellular vesicles (EVs),[3] microvesicles, and exosomes, which serve as vehicles for the transfer of proteins to the sperm surface (1–3). This protein transfer during the interaction of sperm with the microenvironment in the female tract is essential for their maturation and fertilizing ability. In the oviduct where sperm are stored in the sperm reservoir they interact with the alkaline oviductal microenvironment and acquire fertilization factors (4). Consequently, failure of oviductal support has been shown to lead to infertility in mice (5).

Recently, we discovered that the murine oviductal fluid contains EVs, which we termed "oviductosomes" (OVS), and that during the proestrus/estrus stage they carry and deliver to sperm an essential fertility-modulating protein, plasma membrane Ca^{2+}-ATPase 4 (PMCA4) (6). PMCA4 with its two isoforms (4a and 4b), is a 10-pass transmembrane protein that has functional domains on the cytoplasmic side of the membrane and interacts with membrane-associated proteins (7). It is the major Ca^{2+} efflux pump in mouse sperm where it has a higher affinity for Ca^{2+} compared with other Ca^{2+} clearance mechanisms (Na^{+}-Ca^{2+} exchanger (NCX) and mitochondrial Ca^{2+} uniporter (MCU)) (8). Importantly, deletion of *Pmca4* disrupts Ca^{2+} homeostasis and leads to loss of both progressive and hyperactivated sperm motility and ultimately to infertility in mice (9, 10). Earlier, PMCA4 which is expressed in testicular sperm was shown to be synthesized and secreted in the murine epididymis where epididymosomes (extracellular vesicles) were demonstrated to deliver it to sperm *in vitro* (11). Consistent with PMCA4's *in vivo* delivery to epididymal sperm and its crucial role in motility, is the finding of significantly higher levels in caudal sperm compared with caput ones (11), which lack motility (12). This underscores its functional and maturational roles in sperm. Thus, in the female tract the acquisition of

* This work was supported by National Institutes of Health Grant RO3HD073523, National Institutes of Health Grant 5P20RR015588 (to P. A. D.), INBRE Core Access Award (to P. A. D.), and the Saudi Arabian Cultural Mission to USA (to A. A. A.). The authors declare that they have no conflicts of interest with the contents of this article.

[1] Current Address, Dept. of Biology, College of Medicine, University of Dammam (UOD), P.O. Box 2435 Dammam, 31451, Saudi Arabia.
[2] To whom correspondence should be addressed: Dept. of Biological Sciences, University of Delaware, Newark, DE 19716. Tel.: 302-831-2249; Fax: 302-831-2281; E-mail: pdeleon@udel.edu.

[3] The abbreviations used are: EV, extracellular vesicles; OVS, oviductosomes; CAP, capacitation; AR, acrosome reaction; TEM, transmission electron microscopy; VN, vitronectin; FN, fibronectin; OLF, oviductal luminal fluid; HTF, human tubal fluid; SR-SIM, super-resolution structured illumination microscopy; IAM, inner acrosomal membrane.

additional PMCA4 from the OVS might be important for maintaining sperm viability during capacitation (the final sperm maturational stage), as well as in hyperactivation, and acrosome reaction (AR) (6), which all require elevated levels of Ca^{2+} (13–16).

Because OVS are highly likely to play a crucial role in fertility, it is important to determine the mechanism by which they deliver their cargo to the sperm surface. In somatic cells it has been reported that endocytosis and fusion are demonstrated mechanisms for cargo delivery from EVs to recipient cells (17). Since endocytosis does not occur in spermatozoa it is an unlikely mechanism for cargo delivery from OVS or other reproductive EVs. It should be noted that Martin-DeLeon and coworkers (2, 3) have shown that EVs from the epididymal and uterine fluids (epididymosomes and uterosomes, respectively) dock on the sperm membrane in delivering their cargo. They have postulated that from the docked sites hydrophobic interactions may underlie the transfer of glycosyl phosphatidylinositol (GPI)-linked proteins, which are attached to the outer leaflet of the lipid bilayer of the sperm membrane. However, hydrophobic interactions are unlikely to be involved in the transfer of transmembrane proteins, such as PMCA4, which has its catalytic domain on the cytosolic side of the membrane (18).

Recently, Schwarz *et al.* (19) proposed a fusogenic mechanism for the transfer of PMCA4 from epididymosomes to bovine sperm, although the molecular basis underlying the process was not investigated (19). While exosomes/microvesicles are known to carry adhesion molecules such as tetraspanin (CD9 and CD81), which build fusion-competent sites (20, 21), and integrins which play a potential role in cell-to-cell communication (22), the mechanism of their action in cargo delivery remains unknown (23, 24). We hypothesized that cargo delivery from OVS to sperm involves a fusogenic mechanism that is facilitated by fusion-competent sites involving CD9 and integrins on both sperm and OVS.

Thus the goal of this investigation was to use a lipophilic dye and the novel SR-SIM approach that allows three-dimensional imaging with an 8-fold volumetric resolution improvement, compared with state-of-the-art confocal microscopy, to visualize OVS-sperm interaction. Using PMCA4 as a model, and transmission electron microscopy (TEM), we sought to provide evidence for the fusogenic mechanism in cargo delivery from OVS. Our results provide support for the mechanism and reveal that fusion can be blocked by exogenous ligands, fibronectin, and vitronectin, for $\alpha5\beta1$and $\alpha v\beta3$ integrins, their Arg-Gly-Asp recognition motif, and anti-αv antibodies. Thus we provide a schematic model in which we implicate $\alpha5\beta1$ and $\alpha v\beta3$ in the fusion which mediates cargo delivery of OVS during capacitation and after the acrosome reaction. This mechanism is likely to play a role in cargo delivery to sperm from reproductive exosomes and microvesicles, in general.

Materials and Methods

Animals and Reagents—Sexually mature 4–12-week-old female and 10–12-week-old male mice (FVB/N strain; Harlan, Indianapolis, IN) were used throughout the investigation. In addition to these wild-type (WT) mice, *Pmca4*-null mice on the FVBN background were used to provide caudal sperm for the immunofluorescence assays. These mice were a generous gift from Dr. Gary Shull in whose laboratory they were generated (9). Breeding and genotyping of these mice were described previously (9). Studies were approved by the Institutional Animal Care and Use Committee at the University of Delaware and were in agreement with the Guide for the Care and Use of Laboratory Animals published by the National Research Council of the National Academies, 8th Ed., Washington, D.C. (publication 85-23, revised 2011). All enzymes and chemicals were purchased from Fisher Scientific Co., Sigma, or Invitrogen, unless otherwise specified.

Antibodies and Fluorescent Dyes—Rabbit polyclonal antibodies against peptides specific for bovine PMCA4a have been generated and previously validated (25, 26). Sequence analysis suggested a high probability of cross-reactivity with mouse PMCA4a, and studies in mice revealed the specificity of the antibodies for this species (11). Thus these antibodies were used in immunofluorescence microscopy. Goat polyclonal anti-PMCA4 antibody, which detects isoforms 4a and 4b, (SC-22080) and rat monoclonal anti-CD9 antibody (SC-18869) were purchased from Santa Cruz Biotechnology, Dallas, TX. Rabbit polyclonal anti-αv integrin (AB1930) was from Millipore, Temecula, CA. To perform a function-blocking assay, a rat monoclonal antibody against mouse αv integrin subunit (RM47) and its isotype $IgG_{1\kappa}$ (R3–34) were obtained from BD Bioscience (San Diego, CA). Alexa Fluor 405 donkey anti-rabbit (AB175651) was from Abcam, Cambridge, MA. FM4-64FX (F34653) was purchased from Life Technologies, Grand Island, NY. DRAQ5™ (DR05500) was purchased from Biostatus Limited, Leicestershire, UK. Fluoro-Gel (17985–10) and Fluoro-Gel II with DAPI (17985–50) were purchased from Electron Microscope Sciences, Hatfield, PA.

Collection of Oviductal Luminal Fluids from Females after Hormonal Induction of Estrus—Females were induced into estrus as previously described (2, 6). Oviductal luminal fluids (OLF) were obtained from 10 superovulated females per experiment. The methodology of collecting the fluid is similar to that described previously (2, 6).

OVS Preparation—OLF was collected from 10 superovulated females and clarified, as described above. To fractionate the OLF we used a methodology similar to previously described (6). Briefly, the clarified OLF was subjected to ultracentrifugation at 120,000 × *g* for 2 h, at 4 °C using a Beckman Optima 2–70 k ultracentrifuge and a Ti60 rotor. The resulting pellets (OVS), which contain both exosomes and microvesicles, were resuspended in homogenization buffer and protease inhibitor, for Western blot analysis, or in PBS to a final concentration of 1.3 mg/ml proteins to be used for co-incubation with sperm or transmission electron microscopy (TEM).

Preparation of Capacitated and Acrosome-reacted Sperm—Mouse spermatozoa were harvested from the caudal epididymides of 2 sexually mature males per experiment, by mincing the caudae in warm Human Tubal Fluid (HTF, Cat. 2002, *InVitro*Care, Frederick, MD) as described earlier (27) and kept at 37 °C for 10 min to allow sperm to swim out of the tissue. After gravity settling of the tissues, the supernatant was collected. Next, 3.4×10^7 sperm were aliquoted into 1.5-ml tubes (final concentration, 8.5×10^5 sperm) and 100 μl of capacitation

medium (HTF) for 90 min at 37 °C. Calcium ionophore A23187 was added to one aliquot at a final concentration of 20 μM for 60 min of incubation at 37 °C to induce the AR as previously described (28).

Labeling of OVS and Co-incubation of Pre-labeled OVS and Sperm—OVS were collected as described above and resuspended in PBS. The incorporation of FM4–64FX, a lipophilic fluorescent dye into OVS was performed as previously described (3). FM4–64FX (5 mM) was used at 1:100 dilution in the OVS suspension. The mixture was kept at 37 °C overnight. Subsequently, OVS were recovered by ultracentrifugation 120,000 × *g*, 1 h, and washed in PBS. The resulting pellet was resuspended in PBS. 50 μg of FM4–64-FX-labeled OVS was co-incubated with fresh caudal sperm (8.5×10^5 sperm/tube) for 3 h at 37 °C in HTF medium or PBS. Post-coincubation, sperm were washed (4×, 5 min) in PBS at 500 × *g*. The resulting pellet with sperm was used for further analysis (FRAP, SR-SIM, TEM) as described below. Control sperm were incubated in the supernatant penultimate wash for 3 h at 37 °C or directly in FM4–64FX.

Confocal Analysis of Indirect Immunofluorescence Sperm Staining—Immunofluorescence staining was performed as previously described (29, 30). Briefly, capacitated sperm were fixed with 4% paraformaldehyde (cat. 15710, Electron Microscopy Sciences, Hatfield, PA) diluted in PBS for 30 min. After (3×, 5 min) washes in PBS, they were permeabilized with 0.1% Triton X-100 in PBS. They were then washed (3×, 5 min) in PBS, blocked for 30 min in 2% BSA in PBS and then incubated with the primary antibodies (rat anti-CD9 or rabbit anti-αvintegrin, 1:200, 1 h, overnight). Subsequently, they were treated with the appropriate secondary antibodies (1:500 dilution, Alexa Fluor 488 anti-rat or Alexa Fluor 568 anti-rabbit, respectively) for 1 h at room temperature, and washed (4×, 5 min) in PBS and suspensions placed on slides. Following mounting with Fluoro-Gel II containing DAPI, cells were imaged, using a Zeiss LSM 780 confocal microscope. Controls were prepared by replacing primary antibodies with the appropriate IgG isotype.

Co-incubation Assay—Following co-incubation of FM4–64FX-labeled OVS with sperm as described above, samples were post-fixed with 4% paraformaldehyde for 30 min at room temperature, washed with PBS (4×, 5 min), and suspensions placed on slides. Slides were mounted with Fluoro-Gel II with DAPI.

Co-localization of OVS with PMCA4 and αv-Integrin Subunit—After the co-incubation of sperm with FM4–64FX pre-labeled OVS for 3 h, the cells were permeabilized with 0.1% Triton X-100 for 10 min at room temperature. After washing, the cells with blocking buffer (2% BSA in PBS) they were incubated in blocking buffer for 30 min at room temperature. Permeabilized cells were then incubated in rabbit anti-PMCA4a antibody or rabbit anti-αV integrin antibody (1:200 dilution in blocking solution, applied to cells at 4 °C, for 1 h), followed by washing with PBS (3× for 5 min). Next, cells were incubated with the secondary antibody Alexa Fluor 405 donkey anti-rabbit (1:200 dilution) and DRAQ5™ (1:2000 dilution) at room temperature for 1 h. Washed in PBS (4×, 5 min) and suspensions placed on slides, which were mounted with Fluoro-Gel.

SR-SIM Imaging—Images were captured with a 63× Plan-Apochromatic oil immersion objective (numerical aperture of 1.4), using SR-SIM (Zeiss Elyra PSI SIM, Carl Zeiss, Inc., Germany). The FM4–64FX channel was obtained with 488 nm laser excitation and LP 655 nm emission filter. The Alexa Fluor 405 channel was obtained with 405 nm laser excitation and a BP 420–480 nm emission filter; The DAPI channel with 405 nm laser excitation of an Argon laser and band pass (BP) 420–480 nm emission filter; and the DRAQ5 channel with 642 nm laser excitation and a LP 655 nm emission filter. The three-dimensional SR-SIM and Wide-field images were reconstructed with ZEN 2011 (Carl Zeiss, Inc, Germany). Images were generated from z-stacks containing 5 phase shifts and 5 rotations per z-slice (0.091 μm interval) and then processed in the Zen 2011 software. For channel alignment, a multicolored bead slide was imaged using the same image acquisition settings and used for an affine alignment of channels.

Negative Staining for TEM—The methodology of negative staining is similar to previously described (6). Nickel TEM grids (Electron Microscopy Sciences), 400 mesh with a formvar/carbon film, were floated on a drop of the fractions of purified OLF pellet suspension. The grids were then washed with several drops of water and then stained with 1% uranyl acetate, a phospholipid stain, before being subjected to microscopic analysis. Membrane vesicles were imaged using the TEM (Zeiss LIBRA 120).

Pre-embedding Immunogold Labeling for OVS-Sperm Membrane Interaction—The methodology of immunogold labeling is similar to previously described (6, 31). Briefly, after co-incubation for 3 h at 37 °C, the mixture was centrifuged at 500 × *g* for 10 min and resuspended in PBS, and a droplet was applied to a 22-mm round thermanox coverslip coated with poly-L-lysine. Sperm were allowed to adsorb to the surface of the coverslip for 15 min. Samples were then fixed with 4% paraformaldehyde in 0.1 M Sorensens' phosphate buffer, pH 7.2 for 30 min and washed 3× for 15 min each with 0.1 M Sorensens' phosphate buffer, pH 7.2. To inactivate residual aldehyde groups present, coverslips were treated with 0.1% $NaBH_4$ in 0.1 M Sorensens' phosphate buffer (freshly prepared) for 10 min. After, washing 4× for 5 min in 0.1 M Sorensens' phosphate buffer, pH 7.2, sperm were permeabilized with 0.05% Triton X-100 in PBS for 10 min followed with PBS washes, 3× for 10 min. After blocking with AURION Donkey Solution for 30 min, the coverslips containing the sperm sample were incubated with goat anti-PMCA4 diluted 1:50 in BSA-c, overnight at 4 °C. Controls consisted of replacing the primary antibody with normal goat IgG (1:2900 dilution) and replacing the primary antibody with BSA-c. Next day, samples were washed with BSA-c and incubated with donkey anti-goat IgG ultra-small gold-conjugated secondary antibody (800.311, Aurion Immuno Gold Reagents & Accessories, Wageningen, The Netherlands) diluted 1:100 overnight at 4 °C. After being washed with BSA-c and PBS, samples were fixed with 2% glutaraldehyde in 0.1 M Sorensens' phosphate buffer, pH 7.2 for 30 min, washed, and post-fixed with 1% osmium tetroxide (aq) for 15 min. Following extensive water washes, samples were silver enhanced for 20 min using the Aurion R-Gent S.E.-EM silver enhancement kit (500.033, Aurion Immuno Gold Reagents & Accessories, Wageningen,

The Netherlands). Samples were then washed, dehydrated in an ascending acetone series, infiltrated with EMBed-812 epoxy resin, and polymerized at 60 °C overnight. Samples were sectioned on a Reichert Jung UltracutE ultramicrotome, and ultrathin sections were collected onto 200 mesh formvar/carbon-coated nickel grids. Sections were post-stained with methanolic uranyl acetate and Reynolds' lead citrate and imaged on a Zeiss Libra 120 TEM operated at 120kV. Images were acquired with a Gatan Ultrascan 1000 CCD.

SDS-PAGE and Western Blot Analysis—Preparation of protein extracts from OLF and OVS was performed as described previously (6). Proteins from uterus and epididymosomes were used as positive controls. Total protein concentrations in the lysates and OVS were determined using the bicinchoninic acid protein assay kit (Pierce), according to the manufacturer's protocol. Samples for electrophoresis were diluted in 2× Laemmli sample buffer incubated for 5 min at 90 °C. 20 μg of proteins from controls and OVS were loaded per lane on 10% polyacrylamide gels and transferred onto a nitrocellulose membrane (Amersham Biosciences). Western blotting was performed with the WesternBreeze Chemiluminescent Immunodetection Kit (Life Technologies, Grand Island, NY), according to the manufacturer's instructions. Blots were blocked for 1 h at room temperature and incubated in rabbit polyclonal anti-αv integrin primary antibody (1: 500) or in rat monoclonal anti-CD9 primary antibody (1:1000) overnight at 4 °C. Nonspecific binding of antibody was removed using 5× washes of TBST (20 mM Tris, pH 8.0, containing 150 mM NaCl and 0.5% Tween 20) before incubation in the alkaline phosphatase-conjugated anti-rabbit IgG (Invitrogen, diluted 1:2000) or AP-conjugated anti-rat IgG (Sigma-Aldrich, diluted 1:32,000) for 1 h at 4 °C. The membrane was again washed (6×, 15 min) using TBST before chemiluminescence was detected by using the ECL kit (Bio-Rad).

Effect of the Tri-peptide Arg-Gly-Asp (RGD) on OVS-Sperm Fusion—To test the effect of RGD peptide on OVS-sperm membrane fusion, before the *in vitro* assay, either pre-labeled OVS or WT sperm or both were separately pre-incubated for 40 min at 37 °C in HTF medium supplemented with RGD at 1 mM or 1 mg/ml. Then, they were co-incubated in HTF medium at 37 °C for 3 h with final concentration of 8.5×10^5 sperm/tube. After co-incubation sperm were washed (3×, collected with centrifugation at 500 × *g* for 15 min) using PBS. Then they were fixed with 4% paraformaldehyde for 30 min at room temperature, washed (5×, 5 min) with PBS and placed on slides. Slides were mounted with Fluoro-Gel II containing DAPI. Images were captured as described above (see SR-SIM analysis section). A minimum of 33 sperm were analyzed for the number of microvesicles that were unequivocally detectable.

Effect of Fibronectin (FN) or Vitronectin (VN) on OVS-Sperm Fusion—Capacitated sperm (final concentration 8.5×10^5 sperm/tube) were treated with 10 μg/ml FN similarly to that used by Geho *et al.* for platelet adhesion (32) or 0 μg/ml FN (control) for 40 min prior to co-incubation with pre-labeled OVS for 3 h at 37 °C. Acrosome-reacted sperm (final concentration 8.5×10^5 sperm/tube) were treated with 600 nM VN (33) or 0 nM VN (control) for 40 min prior to co-incubation with pre-labeled OVS for 3 h at 37 °C. After co-incubation, sperm were placed on slides and subjected to SR-SIM analysis as described above.

Effect of Anti-αV Antibodies on OVS-Sperm Fusion—Acrosome-reacted sperm and OVS were separately pre-incubated in HTF medium supplemented with 50 μg/ml anti-αv antibodies for 40 min, as previously used to inhibit sperm-oocyte fusion (34). Sperm were then washed and OVS diluted 1:100 in HTF for co-incubation with untreated OVS and sperm, respectively. In parallel, untreated OVS and sperm were co-incubated in the presence of anti-αv antibodies (50 μg/ml) while the control received the same concentration of the IgG isotype. After 3 h co-incubation sperm were washed, fixed, and placed on slides as described above for analysis with SR-SIM. A total of 12 cells were imaged in each of the four groups.

Statistical Analysis—One-way analysis of variance (ANOVA) followed by Tukey-Kramer post hoc was performed on the means ± S.E. for 3 replicates. p values were calculated and *, $p < 0.05$ was considered significant.

Results

Ultrastructure of Murine OVS—Oviductal fluid was collected from females hormonally induced into estrus. Using TEM, the pellet isolated from the oviductal fluid by differential ultracentrifugation was shown to be rich in EVs or OVS (Fig. 1*A*). The OVS consisted of both microvesicles and exosomes (Fig. 1*B*). Immunostaining revealed immunogold particles detecting PMCA4 in the microvesicles (Fig. 1, *C* and *D*) as well as exosomes, as previously shown (6).

In Vitro OVS-Sperm Interaction Was Detected using FM4–64FX Dye and Three-dimensional SR-SIM—To gain insights into the mechanism of delivery of transmembrane proteins to the sperm membrane, a novel experimental approach for the assessment of OVS-sperm interaction was executed, using three-dimensional SR-SIM. OVS pre-labeled with a fluorescent membrane dye, FM4–64FX, and co-incubated with caudal sperm in a co-incubation assay were shown to accumulate on the sperm membrane after 3 h (Fig. 2, *B--F*). Labeled OVS were first detected over the acrosome, followed by other areas on the head, the midpiece (Fig. 2, *B--F*), and the proximal principal piece where they were occasionally seen (data not shown). In addition to the detection of the punctate red signal representing microvesicles, there was continuous decoration of the midpiece with the FM4–64FX red signal. The latter is likely due to the coalescence of exosomes attached to, or fused with, the sperm membrane over the midpiece (Fig. 2*B*). This is in contrast with the negative control sperm samples that were incubated in the supernatant dye solution collected after removing the labeled OVS (Fig. 2*A*). Not only do these control sperm lack the punctate signal on the head, but they also lack the continuous staining on the midpiece, while sperm incubated directly in the dye showed broad labeling over the entire membrane (internal positive control, data not shown).

Co-localization Analysis of OVS and PMCA4a—Immunofluorescence analysis of WT and *Pmca4* KO sperm after co-incubation with pre-labeled OVS revealed co-localization of the OVS with PMCA4a (Fig. 3). Interestingly, three-dimensional SR-SIM allowed us to visualize endogenous PMCA4a molecules located on the inner acrosomal membrane (IAM) (Fig. 3*A*,

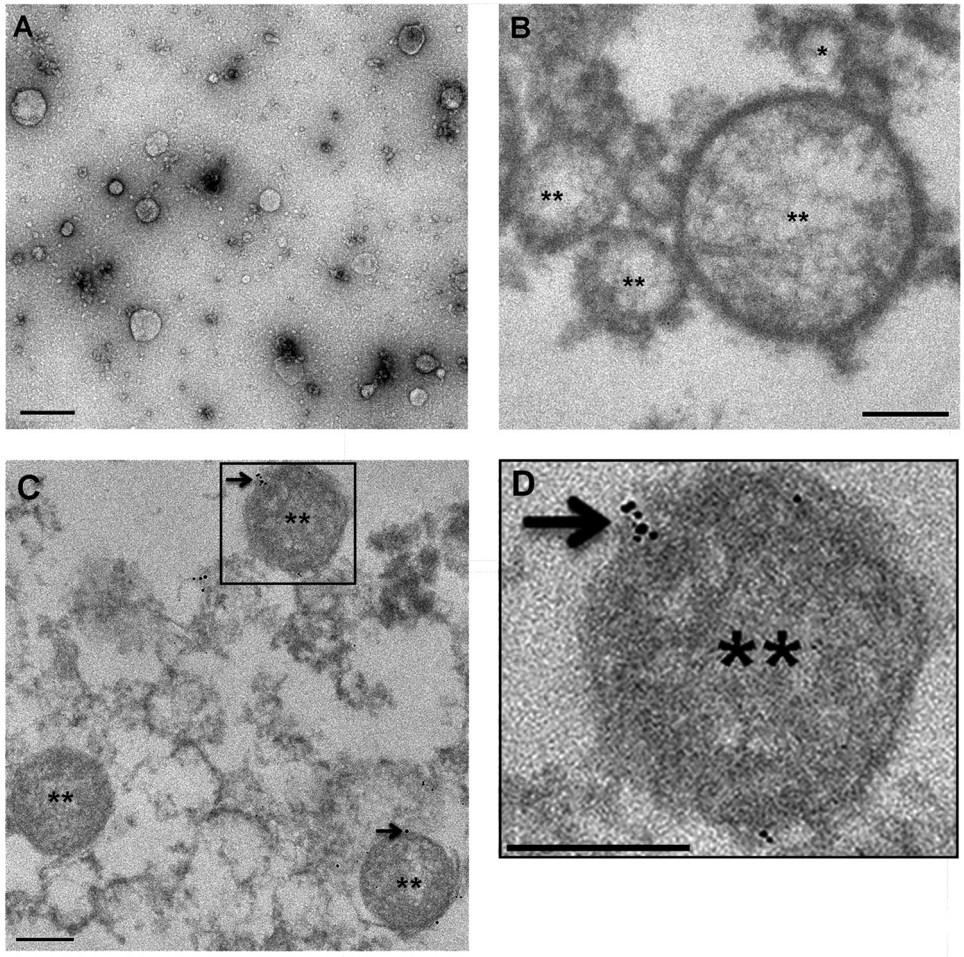

FIGURE 1. **Electron micrographs of mouse OVS.** Oviductosomes, exosomes, and microvesicles, were isolated using differential ultracentrifugation. *A*, overview image of negatively stained samples with uranyl acetate was acquired by transmission electron microscopy. Bar, 100 nm. Immunogold-labeled samples were stained with uranyl acetate, a heavy metal stain that binds to lipids and proteins, prior to imaging with transmission electron microscopy. *B*, microvesicles (**) from IgG control ranged in sizes from 0.1 to 1 μm in diameter and exosomes (*) are $<$ 100 nm, and showed no immunogold particles. *C*, immunogold labeling of PMCA4 (*arrows*) showed ultra-small gold particles on microvesicles (**). *D*, enlarged *inset* of *C*. Images were acquired with a Zeiss. LIBRA 120 TEM at 120 kV. Bar, 200 nm.

c–*d*), identified for the first time. PMCA4a was also detected on the midpiece (Fig. 3, *A* and *B*, *d*–*e*) where it was delivered by both microvesicles and exosomes, as detected by the merging of the green and red signal to give a yellow coloration. This merging is unequivocal in *Pmca4*-null sperm and on the midpiece of WT sperm where endogenous PMCA4 does not reside. We consistently detected an accumulation of signal for endogenous PMCA4a in the posterior head near the neck (Fig. 3*A*, *b*–*d*), and its delivery to *Pmca4*-null sperm via OVS in this region (Fig. 3*B*, *b*–*d*). Prominent PMCA4a signal was detected on the midpiece where it does not reside in mature caudal sperm, suggesting that over time it relocates to the proximal principal piece where lipid rafts exist (35). Importantly, we detected from the FRAP experiment in Fig. 3*C* that OVS are mobile in the sperm plasma membrane, supporting the conclusion that PMCA4a delivered by OVS to the membrane overlying the midpiece translocates to microdomains where it functions. Interestingly, there is evidence to suggest that all OVS do not carry/deliver the identical cargo as some with and without PMCA4a were detected on the plasma membrane over the same sperm head (Fig. 4, *A* and *B*).

Analysis of OVS-Sperm Interaction, using TEM—High magnification TEM analysis was performed to confirm the observations detected by three-dimensional SR-SIM (Fig. 5*A*). Following co-incubation of caudal sperm with unlabeled OVS for 3 h (a period in which large numbers of microvesicles on the sperm membrane and bright continuous staining over the midpiece were detectable, via SR-SIM), sperm were sectioned and immunostained for PMCA4a. Detection of immunogold particles revealed that microvesicles fuse with the sperm plasma membrane in delivering PMCA4a (Fig. 5*B*). Fusion in delivery is seen in three-dimensional SR-SIM where integrated red OVS, on both the membrane over the head (Fig. 5*A*) and the midpiece, merge with the green PMCA4a signal to give a yellow coloration (Fig. 5*C*). Fig. 5*D* demonstrates that not only microvesicles (100–1000 nm), but also exosomes ($<$ 100 nm) fuse with sperm membrane, and their alignment along the membrane in TEM images is consistent with the continuous red signal (Fig. 5*C*) seen with SR-SIM. These results (Fig. 5, *A*–*D*) clearly indicate that OVS fuse with the sperm membrane in the transfer of their constituents, as exemplified by PMCA4 (Fig. 5, *B* and *C*).

CD9 and αv Subunit of αvβ3 of Integrin Are Present on OVS and Caudal Capacitated Sperm Membrane—In an attempt to investigate the molecular interactions underlying the fusion of

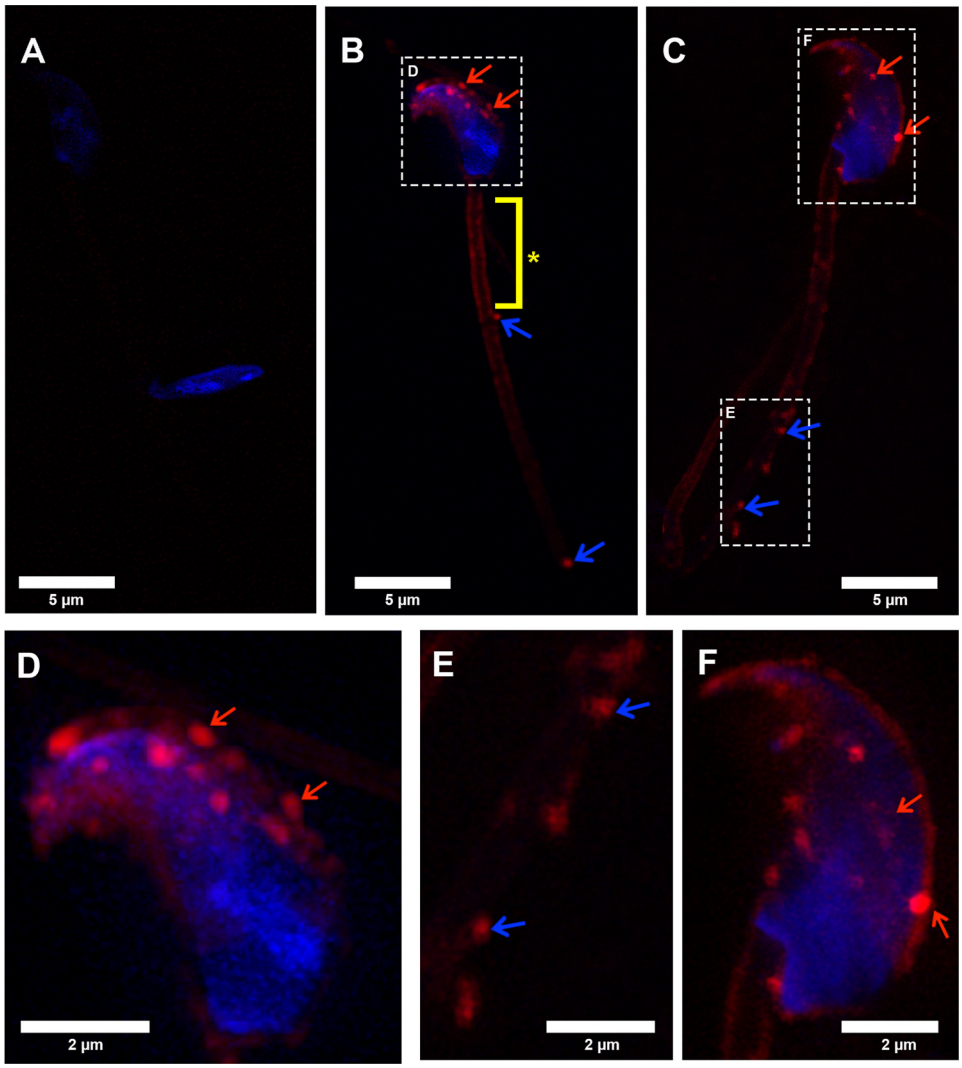

FIGURE 2. **Co-incubation assays detect the transfer of membrane constituents from FM4 – 64FX-labeled OVS to the sperm membrane.** Negative control (*A*) shows the absence of labeling in caudal sperm incubated in supernatant FM4 – 64FX-dye solution. *B* and *C*, labeled OVS (microvesicles) were detected over the acrosome (*red arrows*) and the midpiece (*blue arrows*) after 3 h co-incubation with sperm in PBS. Continuous red staining on the midpiece indicates the OVS (exosomes) fused with the sperm membrane (*). Sperm nuclei were stained *blue* with DAPI. *D* is a magnified view of the *boxed inset* in *B*. *E* and *F* are magnified views of the *boxed insets* in *C*. Representative micrographs shown here are from a total of ~30 sperm imaged. Images were acquired with a 63× Plan-Apochromat oil immersion objective (numerical aperture of 1.4), using SR-SIM. Scale bars, 5 μm.

OVS with sperm membrane, we investigated the presence and localization of CD9 and the αv subunit of αvβ3 integrin, which are known to facilitate membrane fusion (34), on OVS and sperm. Western blotting and indirect immunofluorescence analysis were carried out with anti-CD9 and anti-αv integrin antibodies. Immunofluorescence data showed the presence and distribution patterns of CD9 and αv integrin subunit on the sperm membrane over the head, the midpiece, and on the principal piece. CD9 was less abundant on the plasma membrane over the head than on the flagellum where it was confined primarily to the proximal principal piece (Fig. 6*A*, *a*–*b*). However, the αv integrin subunit extended distally beyond the proximal region of the principal piece (Fig. 6*A*, *c*–*d*). Control sperm samples treated with the IgG isotype gave no signal (Fig. 6*A*, *e*–*f*), confirming the specificity of the antibodies. Western blotting analysis revealed the presence of CD9 (24 kDa) and αv integrin subunit (130 kDa) on OVS from both induced estrus oviductal fluid as well as from spontaneous proestrus/estrus and diestrus/metestrus (Fig. 6*B*). SR-SIM analysis revealed in Fig. 6*C*, *b* the yellow coloration of OVS similar to that seen for the co-localzation of OVS and OVS PMCA4a on the midpiece. However, this coloration cannot unequivocally reflect the co-localization of OVS and OVS αv integrin after *in vitro* fusion with sperm, due to the presence of endogenous αv integrin on the midpiece. Interestingly, endogenous αv integrin subunit was seen on both the head and the principal piece with an accumulation of the signal at the neck (Fig. 6*C*, *b*), similar to PMCA4a (Fig. 3). This spatial relationship of αv integrin and PMCA4a suggests that αvβ3 integrin might be involved in the delivery of PMCA4a to the sperm surface.

Effect of Adhesion Peptide, Arg-Gly-Asp (RGD), for Integrins on OVS-Sperm Fusion—Having demonstrated the presence of αvintegrin subunit on mouse sperm and OVS, we next investigated its involvement in their fusion. We elected to study microvesicles on the sperm membrane instead of exosomes, as the latter were not individually detectable with SR-SIM due to

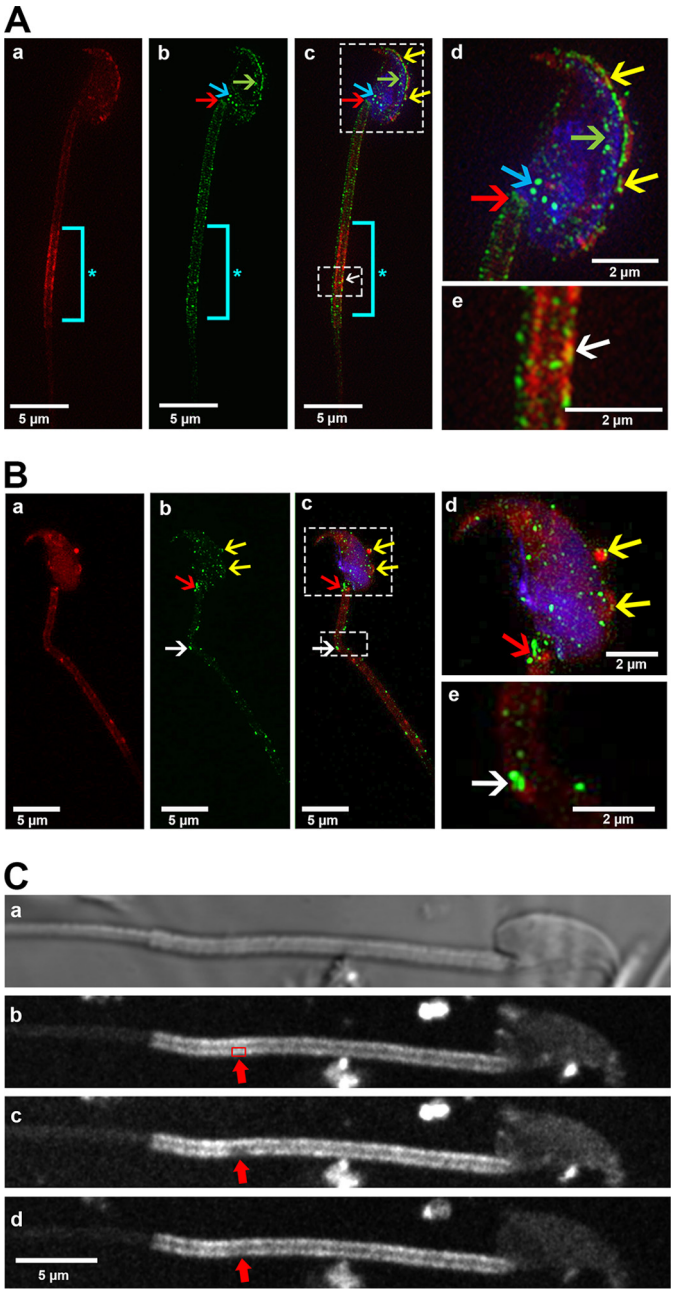

FIGURE 3. **Co-localization of FM4–64FX-labeled OVS and PMCA4a on WT and *Pmca4* KO sperm membrane following co-incubation, as detected by SR-SIM.** *A* and *B*, representative images showing WT (*A*) and *Pmca4* KO (*B*) sperm were incubated with FM4–64FX-labeled OVS. Transferred PMCA4a protein (*green*, *b*, *c*, *d*, *e*) from FM4–64FX-labeled OVS (*red*, *a*, *c*, *d*, *e*) was identified as a co-localized signal (*yellow*) over the acrosome (*yellow arrows*), and on the midpiece (*white arrows*) after the images were merged (*yellow arrows*, *d* and *e*). Endogenous PMCA4a protein was identified for the first time on the inner acrosomal membrane (*A*, *b–d*, *green arrows*) and on the posterior head (*blue arrows*). The neck (*red arrows*) and midpiece (*white arrows*) show PMCA4a staining on the plasma membrane overlying these regions. *, distal midpiece shows intense staining of FM4–64FX-labeled OVS (*aqua bar*). Sperm nuclei were stained with DRAQ5 (*blue*). $n = \sim 18$ sperm in each group. Images were acquired with a 63× Plan-Apochromat oil immersion objective (numerical aperture of 1.4). Scale bars, 5 μm. *C*, fluorescence recovery after photobleaching (FRAP) of FM4–64FX is displayed. FM4–64FX-labeled OVS were incubated with sperm for ~3 h and live sperm were immobilized on poly-L-lysine coated coverglass and imaged with confocal microscopy, which revealed strong staining in the head and midpiece. A representative confocal phase contrast micrograph of a sperm is seen in *a* with the midpiece showing FM4–64FX staining originating from OVS (*b*), before bleaching a specific area (*red box*, *arrowed*) with the 514 nm laser. An image of the bleached area was taken immediately after bleaching (*c*; *red arrow*). Fluorescence recovery proceeded for 9 min. In the bleached area recovery of FM4–64FX is clearly visible (*d*; *red arrow*), suggesting the FM4–64FX is mobile in the membrane. A total of 20 sperm were imaged for the FRAP.

the coalescence of the dye from adjacent vesicles. The average number of microvesicles that fused with sperm in the presence or absence of RGD peptide, the recognition sequence for αv integrin ligand, was determined in four groups. Fig. 7*A* shows that in Group1, the control group, the average number of microvesicles binding to sperm was 18.6. This is significantly different from the 4.7 and 2.8 in Groups 2 and 3, respectively where OVS or sperm was pre-incubated with 1 mM RGD (Fig. 7, *B* and *C*). In Group 4 where both OVS and sperm were separately pre-incubated with 1 mM RGD, the greatest reduction in OVS binding/fusion was seen with a mean of 2 (Fig. 7*D*). ANOVA revealed that Groups (2–4) individually showed significantly reduced OVS-sperm fusion ($p < 0.001$) compared with the control (group 1) (Fig. 7*E*).

Effect of Integrin Ligands, Vitronectin (VN), and Fibronectin (FN), on OVS-Sperm Fusion—To confirm the inhibitory effect of the RGD peptide on OVS-sperm fusion, exogenous ligands (with the RGD interaction motif) for two integrin receptors, $\alpha v\beta 3$ known to be abundantly expressed on the head in acrosome-reacted mouse and human sperm (34, 37) and $\alpha 5\beta 1$ in capacitated human sperm (37, 38), were used to block receptor-ligand interaction in co-incubation assays. When acrosome-reacted and capacitated sperm were co-incubated with exogenous VN and FN, respectively, there was a marked reduction in the number of microvesicles present on the sperm membrane. There was a mean number of 27.7 ± 1.72 on control sperm which differed significantly ($p < 0.001$) from the 17 ± 1.59 seen in the presence of 10 μg/ml FN in the incubation mixture (Fig. 8*A*). For acrosome-reacted sperm in the presence of 0 mM and 600 mM VN, the inhibitory effect was greater with the mean numbers of microvesicles being 32.3 ± 2.18 *versus* 1.03 ± 0.32 ($p < 0.001$) (Fig. 8*B*). It should be noted that microvesicles were detected on both the flagellum and the IAM, indicating that cargo delivery occurs on the sperm head after the AR.

Effect of αv Antibody-blocking on OVS-Sperm fusion—The mean number (2.2 ± 0.36) of microvesicles fused to sperm following co-incubation in the presence of the antibody was significantly lower ($p < 0.0001$), than that in the IgG control (17 ± 2.80) (Fig. 8*C*). To determine the origin of the antibody effect, sperm and OVS were pre-incubated separately with the antibody and both show a similar significant ($p < 0.0001$) reduction in the mean # of fused microvesicles, 2.0 ± 0.51 and 1.9 ± 0.31, as compared with the control (Fig. 8*C*). These data strongly support the involvement of the αv integrin in the fusion of OVS to sperm.

Discussion

The use of nanoscopy or three-dimensional SR-SIM provided new insights on the localization of PMCA4 in different subcellular compartments of murine sperm. To date, PMCA4 has been localized on the membrane over the acrosome and on the proximal principal piece of the flagellum of murine sperm (8–10, 39). In addition to being present over the acrosome, with

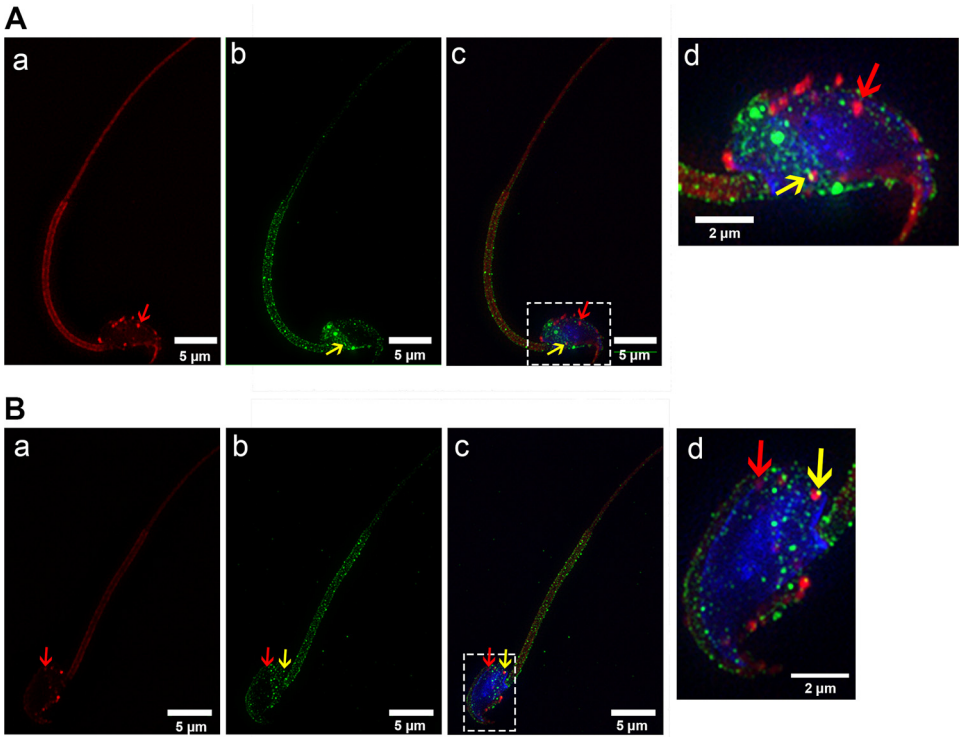

FIGURE 4. **FM4–64FX-labeled OVS carry and deliver different cargoes to sperm following co-incubation, as detected by SR-SIM using PMCA4a as an example.** Two WT sperm (*A*, *B*) are seen (*a*) showing OVS (*red arrow*) and the PMCA4a signal seen in (*b*), while (*c*) shows the merged images. The *inset* in *c* is magnified in *d* where some FM4–64FX-labeled OVS colocalized with PMCA4a (*green*) to yield a yellow signal (*yellow arrow*) and some did not (*red arrow*) indicating the absence of PMCA4a. This observation suggests that OVS carry different cargoes. Sperm nuclei were stained with DRAQ5 (*blue*). Representative images from a total of $n = \sim 18$ sperm. Images were acquired with a 63× Plan-Apochromatic oil immersion objective (numerical aperture of 1.4). Scale bars, 5 μm.

nanoscopy PMCA4 was detected on the IAM, the posterior head, and the neck where the staining often appeared to be intense. Its presence on the IAM and neck may be of physiological relevance. Additional PMCA4 on the IAM would be advantageous to return Ca^{2+} to resting levels after the markedly high influx associated with the AR (14–16, 40), particularly after the loss of PMCA4 molecules on the plasma membrane over the acrosome following this reaction. While the significance of PMCA4 at the neck is not readily apparent, it is known that in human sperm there is a Ca^{2+} store at the neck (41), where PMCA4 immunostaining has been shown to be intense.[4] If such a Ca^{2+} store exists in the neck of the murine sperm, its close proximity to PMCA4 would be parallel to the situation in humans and would highlight the spatially regulated nature of Ca^{2+} signaling.

Evidence for the Fusion of Sperm and OVS Membranes—Sperm analyzed by three-dimensional SR-SIM after incubation with fluorescent-labeled OVS revealed the label predominantly on the head and the midpiece. This distribution of the label is similar to that previously reported on mouse sperm for epididymosomes and uterosomes, with confocal microscopy (3). With three-dimensional SR-SIM we were able to detect distinct punctate, as well as continuous, labeling on the sperm membrane, reflecting the contributions from microvesicles and exosomes, respectively. High magnification TEM analysis of sperm co-incubated with unlabeled OVS confirmed the fusion and contribution of both types of EVs to the sperm plasma membrane, as both could be seen in various stages of attachment to the sperm membrane (Fig. 5, *B* and *D*). These stages include the stalk formation (Fig. 9*c*′), which is a major step in membrane fusion (42).

Prior to fusion, the membrane lipid bilayers must establish close proximity (a distance of < 0.5 nm) within a small area ~ 10 nm (42–44). This will increase the electrostatic repulsion between apposed polar heads of the lipid molecules of the bilayers leading to an opening of the monolayers at the interacting area (Fig. 9). This tension leads to the rupture of the separated monolayers, followed by formation of a stalk and a hydrophilic pore (Fig. 9). The aqueous environment in the hydrophilic pore will lead to the opening of the fusion pore and ultimately downstream fusion stages (42–44). It is known that vesicular curvature enhances fusion (45). Thus it is likely that exosomes with its smaller size and therefore greater curvature would have a greater fusion rate than the larger microvesicles. Our observation of the continuous bright fluorescent label on the midpiece (Figs. 3 and 4) and the close alignment of exosomes on the sperm plasma membrane detected by TEM in this region, as well as on the head (Fig. 5*D*), would be consistent with a greater fusion rate for exosomes on the sperm surface. In general our findings are in support of a fusogenic mechanism consistent with that proposed by Schwarz *et al.* (19) for the transfer of PMCA4 to bovine sperm via epididymosomes.

In addressing the molecular forces that underpin the fusion of OVS and sperm membrane we focused our attention on CD9

[4] Andrews, R. and Martin-DeLeon, P.A., unpublished data.

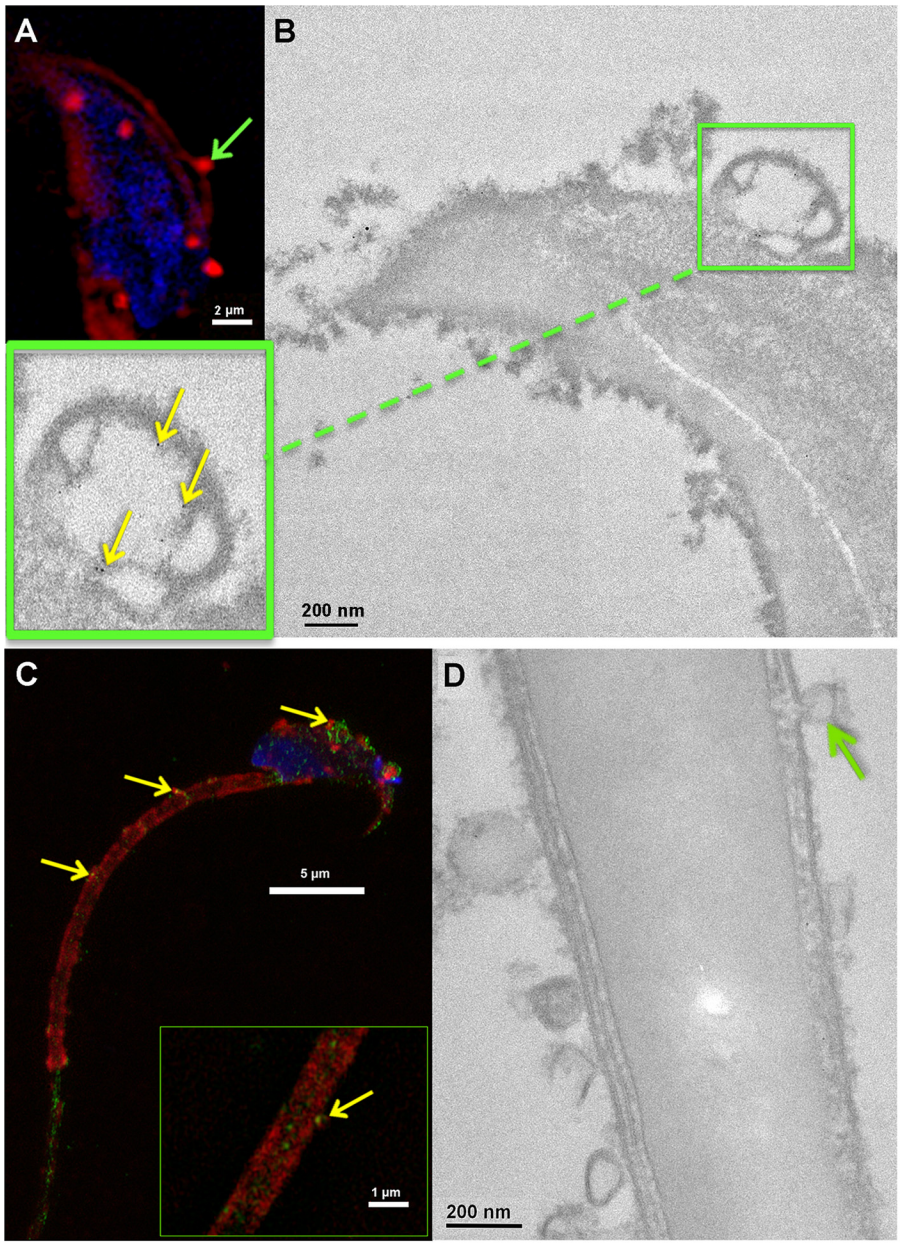

FIGURE 5. **FM4 – 64FX-labeled OVS and immunogold labeling in OVS fused with WT sperm membrane provide evidence for involvement of a fusogenic mechanism in the transfer of PMCA4.** *A*, fusion of a FM4 – 64FX-labeled microvesicle (*green arrow*) with the sperm membrane over the acrosome was seen in SR-SIM images. Sperm nuclei were stained with DRAQ5 (*blue*). In *C*, sperm incubated in labeled OVS acquire the label and PMCA4 (*green signal*) on the plasma membrane overlying the acrosomal cap and the midpiece where the green signal for transferred PMCA4 merges with the red OVS to give yellow (*yellow arrows*). Note that endogenous PMCA4 does not localize to the midpiece. The green staining on the head and the proximal principal piece (*blue arrow*) is the location of endogenous PMCA4. Representative images from a total of $n = \sim 12$ and 18 sperm, respectively. Images were acquired with a 63× Plan-Apochromatic oil immersion objective (numerical aperture of 1.4) *B* and *D*, TEM analysis demonstrates and confirms fusion (*green arrow*). *Inset* shows transfer of gold particles (PMCA4, *yellow arrow*) from OVS to the sperm membrane over the acrosome. Control IgG shows the alignment of OVS along the sperm membrane with the absence of immunogold labeling (*D*). Representative images from a total of $n = \sim 30$ in each group. Images were acquired with a Zeiss. LIBRA 120 TEM at 120kV equipped with a Gatan Ultrascan 1000 CCD camera.

tetraspanin and the αv subunit of αvβ3 integrin. The latter is an adhesion molecule (46, 47) known to be present on the sperm head and to play a role in sperm-oocyte fusion (33, 36). We report for the first time the presence of both CD9 and αv subunit of αvβ3 integrin on the murine sperm flagellum, with the latter extending distally in the principal piece and thereby being more broadly distributed than CD9, which is predominantly on the midpiece (Fig. 6). Interestingly, both of these proteins were earlier shown to be present on the IAM and to increase in abundance after the AR (36, 48). Because we detected that OVS are able to bind to the IAM after the AR, as well as the plasma membrane (Figs. 2 and 8), CD9 and αvβ3 could be temporally and spatially related to OVS on the sperm head. However, their presence on the midpiece and the proximal principal piece to which OVS preferentially bind is relevant to sperm-OVS fusion. Thus we investigated their existence in OVS and show their presence by Western analysis (Fig. 6*B*). Having previously shown the presence of CD9 in OVS by immunoelectron microscopy (6), we confirmed the presence of αv subunit of αvβ3 integrin in OVS, using three-dimensional SR-SIM to

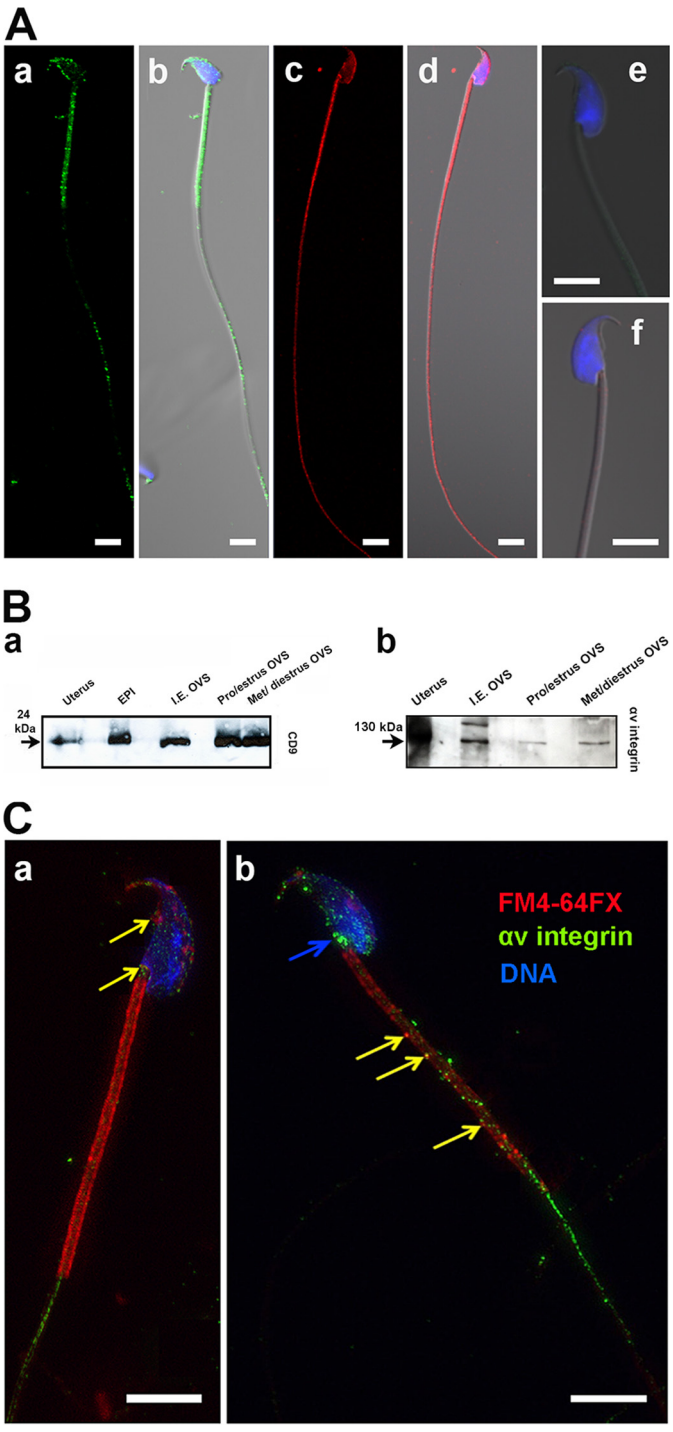

FIGURE 6. **Localization of CD9 and the αv subunit of αvβ3 integrin on sperm and OVS.** *A*, distribution of CD9 and αv integrin on sperm studied by immunofluorescence and conventional confocal microscopy. CD9 (*green*, *a-b*) and αv integrin (*red*, *c-d*) localized on the midpiece, the proximal principal piece, and the over the acrosome. Sperm nuclei were stained with DAPI (*blue*) and are seen in the merged images in *b* and *d*. IgG control did not give any signal (*e-f*).). Representative images from a total of $n = \sim 10$ sperm in each group. *B*, Western blotting analysis performed with anti-CD9 (*a*) and anti-αv integrin (*b*) antibodies on OVS recovered from oviductal fluid, proestrus, and estrus combined and metestrus and diestrus combined, as well as hormonally induced estrus (I.E OVS), using epididymosomes (*EPI*) and uterus as positive controls. The 24-kDa CD9 and the 130-kDa αv integrin are present in OVS from all stages. *C*, co-localization of FM4–64FX-labeled OVS and αv integrin on caudal sperm following co-incubation and *in vitro* fusion, using three-dimensional SR-SIM. Immunofluorescence reveals that transferred αv integrin potentially co-localizes with OVS on the sperm membrane. The localization pattern of αv is similar to PMCA4a, over the acrosome, neck (*blue arrow*), mid-piece, and the proximal principal piece of the sperm flagellum. The *yellow arrows* show potential overlap between the red FM4–64FX and the green αv integrin signal giving yellow on the head (*a*) and on the midpiece (*b*), since the presence of endogenous αv integrin cannot be ruled out at these sites. The green signal on the head (*b*) and principal piece (*a*, *b*) is unequivocally endogenous αv integrin. Sperm nuclei were stained *blue* with DRAQ5. Images were captured with a 63× Plan-Apochromatic oil immersion objective (numerical aperture of 1.4). Representative images from a total of $n = \sim 15$ sperm Scale bars, 5 μm.

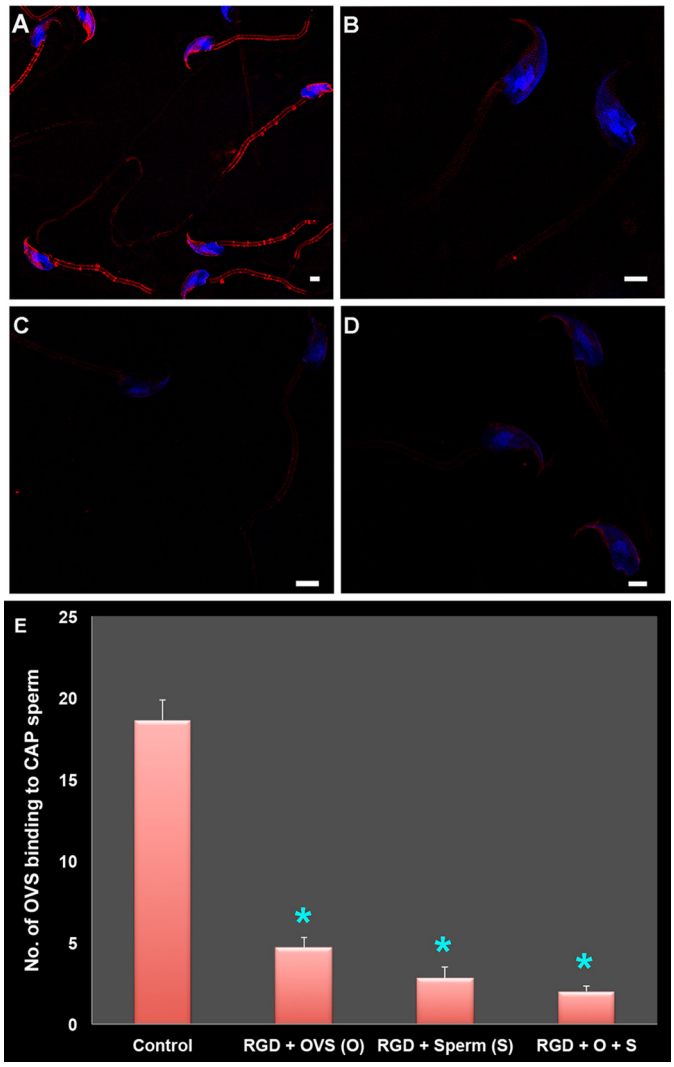

FIGURE 7. **Effect of RGD peptide on mouse OVS-sperm *in vitro* fusion (via co-incubation assays), as assessed in capacitated (CAP) sperm and visualized by SR-SIM.** *A*, control sperm (group 1) acquire pre-FM4–64FX-labeled OVS following co-incubation in the presence of 0 mM RGD. *B–D*, effect of 1 mM RGD peptide on OVS-sperm fusion following pre-incubation of OVS (group 2), sperm (group 3), or both (group 4), respectively, for 40 min at 37 °C is demonstrated. Sperm nuclei were stained *blue* with DAPI. Scale bars, 1 μm. *E*, OVS-sperm fusion was significantly *, $p < 0.001$, inhibited in the presence of RGD in each of the 3 groups (2–4) compare with control (group 1), with the effects appearing to be additive in group 4. Data are presented as the mean (±S.E.) of OVS (microvesicles) per sperm in each group of 33 cells.

detect their co-localization on sperm after their co-incubation (Fig. 6). Thus there is clear evidence that both molecules are present on OVS and sperm at the primary regions where fusion of OVS has been detected.

To detect a functional involvement of αvβ3 integrin in sperm-OVS interaction and to support our hypothesis of a

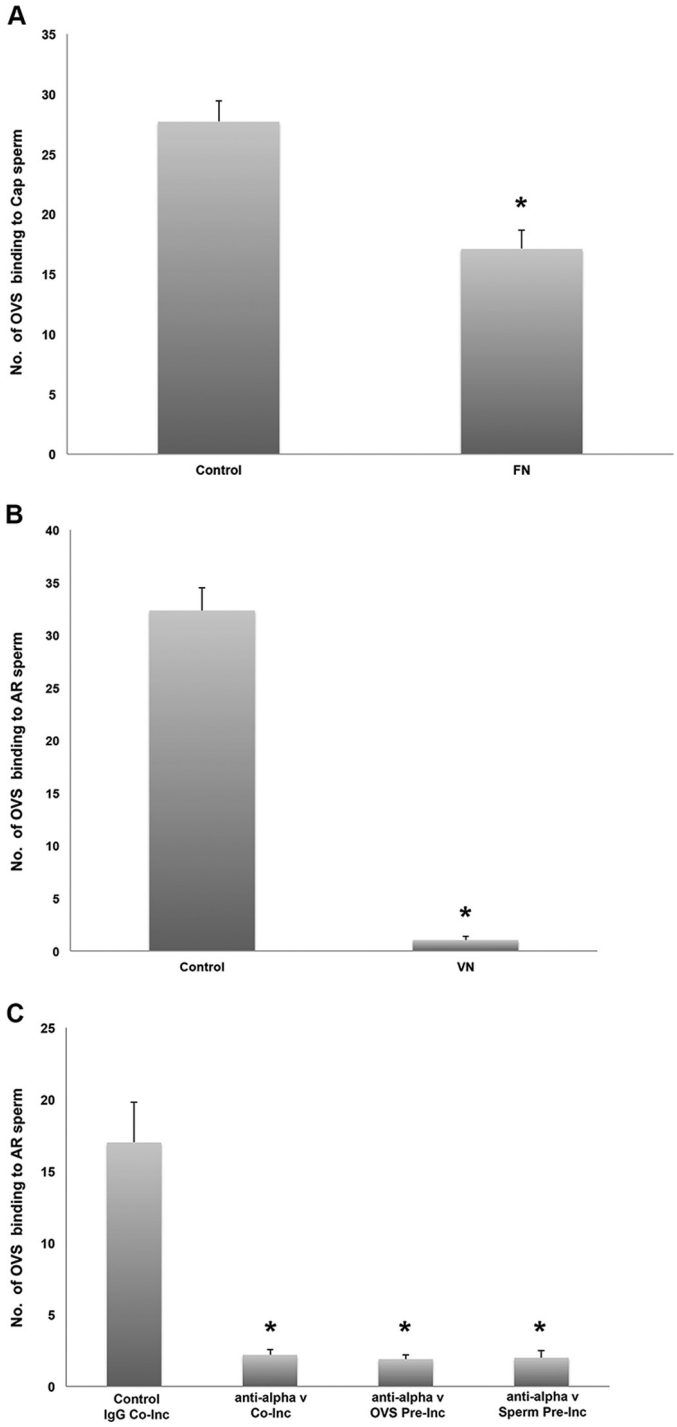

FIGURE 8. **Effect of FN, VN, and anti-αv antibodies on mouse OVS-sperm *in vitro* fusion (via co-incubation assays), as assessed by SR-SIM.** Fusion rate or mean (±S.E.) numbers of OVS (microvesicles) that were fused with capacitated (CAP, *A*) or acrosome-reacted (AR; *B*, *C*) sperm were calculated following co-incubation of pre-FM4–64FX-labeled OVS and sperm in HTF medium supplemented with *B*, 10 μg/ml FN or 600 nM VN, respectively, and *C*, 50 μg/ml of anti-αv antibodies for 3 h at 37 °C in the dark. Isotype IgG and anti-αv antibodies were added during the co-incubation (Co-Inc) for control and test, respectively, while either OVS or sperm were pre-incubated (Pre-Inc) with the antibody prior to coincubation. Data presented as the mean (±S.E.) of OVS per sperm in each group, consisting of 33 cells in *A* and *B* and in *C* at least 10 of the 12 cells imaged. *, values are significantly different from control with 0 μg/ml FN ($p < 0.001$) or 0 nM VN ($p < 0.001$), or Isotype IgG ($p < 0.0001$).

fusogenic mechanism, we used a receptor-ligand blocking assay as well as an antibody-blocking assay to investigate fusion. Both vitronectin, the ligand for αvβ3, and its RGD tripeptide with which it interacts with its receptor were able to significantly block sperm-OVS fusion (Figs. 7 and 8). A significant inhibitory effect was also seen when the anti-αv subunit was used to block the integrin receptor on either the sperm or the OVS, confirming the involvement of integrin in the fusion process. A similar anti-αv inhibitory effect has been reported for mouse sperm in IVF with the identical antibody concentration used in the present study (34).

An inhibitory effect was also seen when fibronectin, the ligand for α5β1 integrin, which is known to be increased on both human and mouse capacitated sperm (37, 49), was added to the co-incubation assay with capacitated sperm (Fig. 8*A*). These findings indicate that integrins, specifically αvβ3 and α5β1, and their ligands play an important role in OVS-sperm interaction and fusion, as they do in sperm head-oocyte fusion (34). It should be noted that in bovine IVF exogenous vitronectin has been shown to have a dual concentration-dependent effect, enhancing sperm penetration at low concentrations (10–100 nM) while having an inhibitory effect at high (500 nM-1 μM) concentrations (33) which include that used in the present study.

Since it has been shown that mammalian sperm express fibronectin and vitronectin and their respective receptors, α5β1 and αvβ3 integrins at their surface after capacitation and AR (33, 37, 49), our data provide support for a receptor-ligand interaction in sperm-OVS fusion on both the sperm head and the flagellum (midpiece). Based on the finding that the antagonistic effect of the RGD blocking on both the sperm and the OVS appeared to be additive, compared with blocking each separately (Fig. 7) as well as the analogous receptor-ligand interaction reported for sperm-oocyte interaction (34), we propose a schematic model in Fig. 9. In this model we show the involvement of CD9 which acts as a scaffold protein (50) to tether adhesion molecules such as αvβ3 integrin (50), with which it co-localizes on sperm, and α5β1. During capacitation and the AR when OVS are released and the ligands and their receptors are increased on sperm (37, 38), receptor-ligand interactions are favored and facilitate fusion. However, as mentioned above, in the presence of exogenous ligand in high concentrations, fusion will be inhibited as seen in Fig. 8. This inhibition is considered to be due partly to compromised membrane integrity (33). In the case of vitronectin, the inhibitory effect may involve multimerization of several molecules (33) which in our model would lengthen the interconnecting bridge and prevent the membranes from coming close enough to form a fusion tube.

Delivery of Transmembrane Proteins to the Sperm Surface via Membrane Fusion—We have previously provided evidence that murine epididymal sperm are able to acquire PMCA4, a ten-pass transmembrane protein, during their maturation as they travel from the caput to the cauda and that epididymosomes can deliver it to caudal sperm *in vitro* (11). Similar findings were obtained for bovine sperm and epididymosomes (19), and OVS were also shown to deliver PMCA4 *in vitro* to murine sperm (6). In this study, we show co-immunolocalization of PMCA4 and

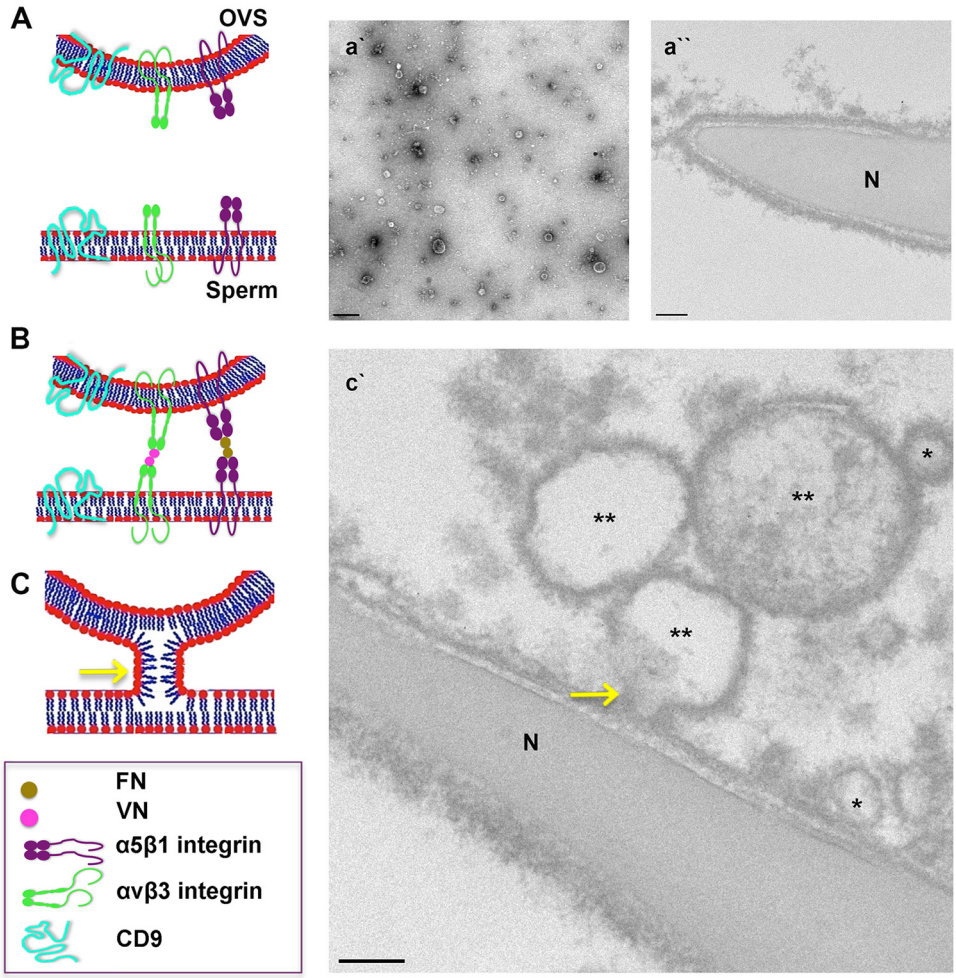

FIGURE 9. **Schematic model showing molecular interactions in OVS-sperm fusion.** *A*, CD9 generates fusion-competent sites on the membranes of both the OVS and the sperm. OVS (a′) and sperm membrane (a″) carry adhesion proteins such as $\alpha5\beta1$and $\alpha v\beta3$ integrins. *B*, respective ligands for these integrins, FN and VN bind to their activated receptor upon capacitation and acrosome reaction, respectively. These integrins facilitate the adhesion of the two membranes by bringing them close together. *C*, close proximity of the membranes leads to electrostatic repulsion between the apposed polar heads of the lipids and the opening of the outer leaflets of the membranes resulting in a fusion stalk formation (c′, *yellow arrow*). Transmission electron micrographs (a′, a″, c′) support the proposed model of membrane fusion. *n* = nucleus; *, exosomes (size < 100 nm); **, microvesicles (size ranging from 100 nm to 1 μm). Bar represents 200 nm.

fluorescently-labeled OVS that were fused to the sperm surface, providing evidence that OVS deliver their cargo via fusion. TEM confirmed that microvesicles, like exosomes (6), carry and deliver PMCA4 to sperm. Interestingly, we detected fusion and delivery of PMCA4 to be predominant on the midpiece, a location where it has not been reported in caudal sperm where it is found on the proximal principal piece in addition to being over the acrosome (8–10, 39). The plasma membrane over the proximal principal piece and the acrosome in murine sperm are known to be lipid rafts microdomains (35, 51), which are locations where PMCA4 is found in somatic cells (52) and where signal transduction occurs (53). It is likely that there is subsequent rearrangement of these microdomains to re-position PMCA4 in lipid rafts (54), or, as shown from the FRAP experiment, the mobility of OVS in the sperm membrane is responsible for the relocation of PMCA4 after delivery.

In addition to PMCA4, we have observed that the αv subunit of $\alpha v\beta3$ integrin, a transmembrane protein could potentially be also delivered to sperm, as merging of the fluorescent signals for OVS and αv could be detected on sperm following co-incubation (Fig. 6). As mentioned earlier this merging of color could also be due to the endogenous protein. Since $\alpha v\beta3$ is an important sperm protein involved in sperm-oocyte fusion (34), it seems clear that sperm-OVS fusion plays an important role in delivering transmembrane and other membrane-associated proteins to sperm during their final maturational period. It should be noted that since PMCA4 is also delivered by epididymosomes (11, 19) and by human prostasomes,[4] these EVs are likely to use the same receptor-ligand interaction to facilitate fusion.

In conclusion we have exploited the power of three-dimensional SR-SIM and high magnification TEM to show that microvesicles and exosomes fuse with the sperm membrane in delivering their cargo, with exosomes appearing to be more efficient in fusing. Fusion can be inhibited by blocking receptor-ligand binding via antibodies or exogenous ligands and their RGD recognition peptide for interaction with sperm integrins, known to play a role in sperm-oocyte fusion. While detecting fusion and delivery of PMCA4 and likely $\alpha v\beta3$ (via the αv subunit), which are transmembrane proteins, we also fine-tuned the subcellular localization of PMCA4 in murine sperm, by showing its presence on the posterior head, the neck, and the

IAM where it is physiologically relevant after the AR. The mechanism uncovered here is likely to be also involved in cargo delivery of prostasomes, epididymosomes, and uterosomes.

Acknowledgments—We thank Dr. Emanuel E. Strehler from the Department of Biochemistry, Mayo Clinic for his generous gift of PMCA4a antibody. We thank Dr. Gary E. Shull from Molecular Genetics, Biochemistry, and Microbiology, The University of Cincinnati College of Medicine, for the kind gift of the Pmca4 knock-out mice.

References

1. Caballero, J., Frenette, G., and Sullivan, R. (2011) Post testicular sperm maturational changes in the bull: important role of the epididymosomes and prostasomes. *Vet. Med. Int.* **2011,** 757194
2. Griffiths, G. S., Galileo, D. S., Aravindan, R. G., and Martin-DeLeon, P. A. (2009) Clusterin facilitates exchange of glycosyl phosphatidylinositol-linked SPAM1 between reproductive luminal fluids and mouse and human sperm membranes. *Biol. Reprod.* **81,** 562–570
3. Griffiths, G. S., Galileo, D. S., Reese, K., and Martin-DeLeon, P. A. (2008) Investigating the role of murine epididymosomes and uterosomes in GPI-linked protein transfer to sperm using SPAM1 as a model. *Mol. Reprod. Dev.* **75,** 1627–1636
4. Coy, P., Garcia-Vázquez, F. A., Visconti, P. E., and Avilés, M. (2012) Roles of the oviduct in mammalian fertilization. *Reproduction* **144,** 649 – 660
5. Hong, X., Luense, L. J., McGinnis, L. K., Nothnick, W. B., and Christenson, L. K. (2008) Dicer1 is essential for female fertility and normal development of the female reproductive system. *Endocrinology* **149,** 6207– 6212
6. Al-Dossary, A. A., Strehler, E. E., and Martin-DeLeon, P. A. (2013) Expression and secretion of plasma membrane Ca2+-ATPase 4a (PMCA4a) during murine estrus: association with oviductal exosomes and uptake in sperm. *PloS one* **8,** e80181
7. Strehler, E. E., and Zacharias, D. A. (2001) Role of alternative splicing in generating isoform diversity among plasma membrane calcium pumps. *Physiol. Rev.* **81,** 21–50
8. Wennemuth, G., Babcock, D. F., and Hille, B. (2003) Calcium clearance mechanisms of mouse sperm. *J. Gen. Physiol.* **122,** 115–128
9. Okunade, G. W., Miller, M. L., Pyne, G. J., Sutliff, R. L., O'Connor, K. T., Neumann, J. C., Andringa, A., Miller, D. A., Prasad, V., Doetschman, T., Paul, R. J., and Shull, G. E. (2004) Targeted ablation of plasma membrane Ca2+-ATPase (PMCA) 1 and 4 indicates a major housekeeping function for PMCA1 and a critical role in hyperactivated sperm motility and male fertility for PMCA4. *J. Biol. Chem.* **279,** 33742–33750
10. Schuh, K., Cartwright, E. J., Jankevics, E., Bundschu, K., Liebermann, J., Williams, J. C., Armesilla, A. L., Emerson, M., Oceandy, D., Knobeloch, K. P., and Neyses, L. (2004) Plasma membrane Ca2+ ATPase 4 is required for sperm motility and male fertility. *J. Biol. Chem.* **279,** 28220 –28226
11. Patel, R., Al-Dossary, A. A., Stabley, D. L., Barone, C., Galileo, D. S., Strehler, E. E., and Martin-DeLeon, P. A. (2013) Plasma membrane Ca2+-ATPase 4 in murine epididymis: secretion of splice variants in the luminal fluid and a role in sperm maturation. *Biol. Reprod.* **89,** 6
12. Yeung, C. H., and Cooper, T.G. (2002) Acquisition and development of sperm motility upon maturation in the epididymis in The Epididymis: From Molecules to Clinical Practice (Robaire, B., Hinton, B. T., ed), pp. 417— 434; Kluwer Academic/Plenum Publishers, New York, NY
13. Gadella, B. M., and Luna, C. (2014) Cell biology and functional dynamics of the mammalian sperm surface. *Theriogenology* **81,** 74 – 84
14. Ho, H. C., Granish, K. A., and Suarez, S. S. (2002) Hyperactivated motility of bull sperm is triggered at the axoneme by Ca2+ and not cAMP. *Dev. Biol.* **250,** 208 –217
15. Ho, H. C., and Suarez, S. S. (2003) Characterization of the intracellular calcium store at the base of the sperm flagellum that regulates hyperactivated motility. *Biol. Reprod.* **68,** 1590 –1596
16. Suarez, S. S., and Ho, H. C. (2003) Hyperactivation of mammalian sperm. *Cell Mol. Biol.* **49,** 351–356
17. Raposo, G., and Stoorvogel, W. (2013) Extracellular vesicles: exosomes, microvesicles, and friends. *J. Cell Biol.* **200,** 373–383
18. Strehler, E. E., Filoteo, A. G., Penniston, J. T., and Caride, A. J. (2007) Plasma-membrane Ca(2+) pumps: structural diversity as the basis for functional versatility. *Biochem. Soc. Trans.* **35,** 919 –922
19. Schwarz, A., Wennemuth, G., Post, H., Brandenburger, T., Aumüller, G., and Wilhelm, B. (2013) Vesicular transfer of membrane components to bovine epididymal spermatozoa. *Cell Tissue Res.* **353,** 549 –561
20. Théry, C., Ostrowski, M., and Segura, E. (2009) Membrane vesicles as conveyors of immune responses. *Nature Reviews. Immunology* **9,** 581–593
21. Théry, C., Zitvogel, L., and Amigorena, S. (2002) Exosomes: composition, biogenesis and function. *Nature Reviews. Immunology* **2,** 569 –579
22. Gille, J., and Swerlick, R. A. (1996) Integrins: role in cell adhesion and communication. *Ann. N.Y. Acad. Sci.* **797,** 93–106
23. Maecker, H. T., Todd, S. C., and Levy, S. (1997) The tetraspanin superfamily: molecular facilitators. *FASEB J.* **11,** 428 – 442
24. Hemler, M. E. (1998) Integrin associated proteins. *Curr. Opin. Cell Biol.* **10,** 578 –585
25. Brandenburger, T., Strehler, E. E., Filoteo, A. G., Caride, A. J., Aumüller, G., Post, H., Schwarz, A., and Wilhelm, B. (2011) Switch of PMCA4 splice variants in bovine epididymis results in altered isoform expression during functional sperm maturation. *J. Biol. Chem.* **286,** 7938 –7946
26. Filoteo, A. G., Elwess, N. L., Enyedi, A., Caride, A., Aung, H. H., and Penniston, J. T. (1997) Plasma membrane Ca2+ pump in rat brain. Patterns of alternative splices seen by isoform-specific antibodies. *J. Biol. Chem.* **272,** 23741–23747
27. Chen, H., Griffiths, G., Galileo, D. S., and Martin-DeLeon, P. A. (2006) Epididymal SPAM1 is a marker for sperm maturation in the mouse. *Biol. Reprod.* **74,** 923–930
28. Deng, X., Czymmek, K., and Martin-DeLeon, P. A. (1999) Biochemical maturation of Spam1 (PH-20) during epididymal transit of mouse sperm involves modifications of N-linked oligosaccharides. *Mol. Reprod. Dev.* **52,** 196 –206
29. Modelski, M. J., Menlah, G., Wang, Y., Dash, S., Wu, K., Galileo, D. S., and Martin-DeLeon, P. A. (2014) Hyaluronidase 2: A Novel Germ Cell Hyaluronidase with Epididymal Expression and Functional Roles in Mammalian Sperm. *Biol. Reprod.* **91,** 109
30. Reese, K. L., Aravindan, R. G., Griffiths, G. S., Shao, M., Wang, Y., Galileo, D. S., Atmuri, V., Triggs-Raine, B. L., and Martin-DeLeon, P. A. (2010) Acidic hyaluronidase activity is present in mouse sperm and is reduced in the absence of SPAM1: evidence for a role for hyaluronidase 3 in mouse and human sperm. *Mol. Reprod. Dev.* **77,** 759 –772
31. Pisitkun, T., Shen, R. F., and Knepper, M. A. (2004) Identification and proteomic profiling of exosomes in human urine. *Proc. Natl. Acad. Sci. U.S.A.* **101,** 13368 –13373
32. Geho, D. H., Smith, W. I., Jr., Liotta, L. A., and Roberts, D. D. (2003) Fibronectin-based masking molecule blocks platelet adhesion. *Bioconjug. Chem.* **14,** 703–706
33. Thys, M., Nauwynck, H., Vandaele, L., Bijttebier, J., Maes, D., Favoreel, H., and Van Soom, A. (2012) Vitronectin and Its Receptor (Integrin $\alpha v\beta 3$) During Bovine Fertilization In Vitro, in A Bird's-Eye View of Veterinary Medicine (Perez-Marin, C. C., ed), pp. 503–522, ISBN: 978-953-51-0031-7, InTech, Croatia, Europe. DOI: 10.5772/37408
34. Boissonnas, C. C., Montjean, D., Lesaffre, C., Auer, J., Vaiman, D., Wolf, J. P., and Ziyyat, A. (2010) Role of sperm $\alpha v\beta 3$ integrin in mouse fertilization. *Dev. Dyn.* **239,** 773–783
35. Travis, A. J., Merdiushev, T., Vargas, L. A., Jones, B. H., Purdon, M. A., Nipper, R. W., Galatioto, J., Moss, S. B., Hunnicutt, G. R., and Kopf, G. S. (2001) Expression and localization of caveolin-1, and the presence of membrane rafts, in mouse and Guinea pig spermatozoa. *Dev. Biol.* **240,** 599 – 610
36. Hemler, M. E. (2003) Tetraspanin proteins mediate cellular penetration, invasion, and fusion events and define a novel type of membrane microdomain. *Annu. Rev. Cell Dev. Biol.* **19,** 397– 422
37. Fusi, F. M., Tamburini, C., Mangili, F., Montesano, M., Ferrari, A., and Bronson, R. A. (1996) The expression of αv, $\alpha 5$, $\beta 1$, and $\beta 3$ integrin chains on ejaculated human spermatozoa varies with their functional state. *Mol. Hum. Reprod.* **2,** 169 –175
38. Bronson, R. A., and Fusi, F. M. (1996) Integrins and human reproduction.

Mol. Hum. Reprod. **2,** 153–168
39. Aravindan, R. G., Fomin, V. P., Naik, U. P., Modelski, M. J., Naik, M. U., Galileo, D. S., Duncan, R. L., and Martin-DeLeon, P. A. (2012) CASK interacts with PMCA4b and JAM-A on the mouse sperm flagellum to regulate Ca2+ homeostasis and motility. *J. Cell. Physiol.* **227,** 3138–3150
40. O'Toole, C. M., Arnoult, C., Darszon, A., Steinhardt, R. A., and Florman, H. M. (2000) Ca(2+) entry through store-operated channels in mouse sperm is initiated by egg ZP3 and drives the acrosome reaction. *Mol. Biol. Cell* **11,** 1571–1584
41. Costello, S., Michelangeli, F., Nash, K., Lefievre, L., Morris, J., Machado-Oliveira, G., Barratt, C., Kirkman-Brown, J., and Publicover, S. (2009) Ca2+-stores in sperm: their identities and functions. *Reproduction* **138,** 425–437
42. Kozlov, M. M., Leikin, S. L., Chernomordik, L. V., Markin, V. S., and Chizmadzhev, Y. A. (1989) Stalk mechanism of vesicle fusion. Intermixing of aqueous contents. *Eur. Biophys.* **17,** 121–129
43. Leikin, S. L., Kozlov, M. M., Chernomordik, L. V., Markin, V. S., and Chizmadzhev, Y. A. (1987) Membrane fusion: overcoming of the hydration barrier and local restructuring. *J. Theor. Biol.* **129,** 411–425
44. Chernomordik, L. V., and Kozlov, M. M. (2003) Protein-lipid interplay in fusion and fission of biological membranes. *Annu. Rev. Biochem.* **72,** 175–207
45. Pencer, J., Jackson, A., Kucerka, N., Nieh, M. P., and Katsaras, J. (2008) The influence of curvature on membrane domains. *Eur. Biophys. J.* **37,** 665–671
46. Seftor, R. E., Seftor, E. A., Gehlsen, K. R., Stetler-Stevenson, W. G., Brown, P. D., Ruoslahti, E., and Hendrix, M. J. (1992) Role of the αv β3 integrin in human melanoma cell invasion. *Proc. Natl. Acad. Sci. U.S.A.* **89,** 1557–1561
47. Danen, E. H., Ten Berge, P. J., Van Muijen, G. N., Van 't Hof-Grootenboer, A. E., Bröcker, E. B., and Ruiter, D. J. (1994) Emergence of α5 β1 fibronectin- and αv β3 vitronectin-receptor expression in melanocytic tumour progression. *Histopathology* **24,** 249–256
48. Ito, C., Yamatoya, K., Yoshida, K., Maekawa, M., Miyado, K., and Toshimori, K. (2010) Tetraspanin family protein CD9 in the mouse sperm: unique localization, appearance, behavior and fate during fertilization. *Cell Tissue Res.* **340,** 583–594
49. Fusi, F. M., Lorenzetti, I., Vignali, M., and Bronson, R. A. (1992) Sperm surface proteins after capacitation. Expression of vitronectin on the spermatozoan head and laminin on the sperm tail. *J. Androl.* **13,** 488–497
50. Peddibhotla, S. S., Brinkmann, B. F., Kummer, D., Tuncay, H., Nakayama, M., Adams, R. H., Gerke, V., and Ebnet, K. (2013) Tetraspanin CD9 links junctional adhesion molecule-A to alphavbeta3 integrin to mediate basic fibroblast growth factor-specific angiogenic signaling. *Mol. Biol. Cell* **24,** 933–944
51. Asano, A., Selvaraj, V., Buttke, D. E., Nelson, J. L., Green, K. M., Evans, J. E., and Travis, A. J. (2009) Biochemical characterization of membrane fractions in murine sperm: identification of three distinct sub-types of membrane rafts. *J. Cell Physiol.* **218,** 537–548
52. Sepúlveda, M. R., Berrocal-Carrillo, M., Gasset, M., and Mata, A. M. (2006) The plasma membrane Ca2+-ATPase isoform 4 is localized in lipid rafts of cerebellum synaptic plasma membranes. *J. Biol. Chem.* **281,** 447–453
53. Sleight, S. B., Miranda, P. V., Plaskett, N. W., Maier, B., Lysiak, J., Scrable, H., Herr, J. C., and Visconti, P. E. (2005) Isolation and proteomic analysis of mouse sperm detergent-resistant membrane fractions: evidence for dissociation of lipid rafts during capacitation. *Biol. Reprod.* **73,** 721–729
54. Cross, N. L. (2004) Reorganization of lipid rafts during capacitation of human sperm. *Biol. Reprod.* **71,** 1367–1373